Structural and optical properties of Mg_2NiH_x switchable mirrors upon hydrogen loading

W. Lohstroh,[1,*] R. J. Westerwaal,[1] J. L. M. van Mechelen,[1] C. Chacon,[2] E. Johansson,[2] B. Dam,[1] and R. Griessen[1]
[1]*Faculty of Sciences, Department of Physics and Astronomy, Condensed Matter Physics, Vrije Universiteit, De Boelelaan 1081, 1081 HV Amsterdam, The Netherlands*
[2]*Department of Physics, Uppsala University, 751 21 Uppsala, Sweden*
(Received 27 April 2004; published 18 October 2004)

The structural, thermodynamic and optical properties of Mg_2Ni thin films covered with Pd are investigated upon exposure to hydrogen. Similar to bulk, thin films of metallic Mg_2Ni take up 4 hydrogen per formula unit and semiconducting transparent $Mg_2NiH_{4-\delta}$ is formed. The dielectric function $\tilde{\epsilon}$ of Mg_2Ni and fully loaded $Mg_2NiH_{4-\delta}$ is determined from reflection and transmission measurements using a Drude-Lorentz parametrization. Besides the two "normal" optical states of a switchable mirror—metallic reflecting and semiconducting transparent—Mg_2NiH_x exhibit a third "black" state at intermediate hydrogen concentrations with low reflection and essentially zero transmission. This state originates from a subtle interplay of the optical properties of the constituent materials and a self-organized double layering of the film during loading. $Mg_2NiH_{4-\delta}$ preferentially nucleates at the film/substrate interface and not—as intuitively expected—close to the catalytic Pd capping layer. Using $\tilde{\epsilon}_{Mg_2Ni}$ and $\tilde{\epsilon}_{Mg_2NiH_4}$ and this loading sequence, the optical response at all hydrogen concentrations can be described quantitatively. The uncommon hydrogen loading sequence is confirmed by x-ray diffraction and hydrogen profiling using the resonant nuclear reaction $^1H(^{15}N,\alpha\gamma)^{12}C$. Pressure-composition isotherms suggest that the formation of $Mg_2NiH_{4-\delta}$ at the film/substrate interface is mainly due to locally enhanced kinetics.

DOI: 10.1103/PhysRevB.70.165411 PACS number(s): 78.20.−e, 68.55.−a, 78.40.−q, 82.47.−a

I. INTRODUCTION

The discovery of the spectacular optical changes of yttrium and lanthanum thin films upon reversible hydrogen absorption by Huiberts *et al.* in 1996,[1] also demonstrated that materials which are reduced to powder when hydrogenated in bulk form, remain structurally intact as a thin film. This offers the opportunity to investigate the intrinsic physical properties of these materials. Since 1996, it has been demonstrated that all rare earth metals (first generation switchable mirrors) and their alloys with Mg (second generation)[2] switch optically upon hydrogen absorption. Richardson *et al.* found that Mg_2NiH_x and other Mg-TM-hydrides (TM: transition metals Co, Fe, Mn) also change reversibly from a metallic to a transparent state upon hydrogen absorption (third generation switchable mirrors).[3,4]

Bulk Mg_2Ni absorbs hydrogen in solid solution up to $x \approx 0.3$. Above $x \approx 0.3$ a semiconducting complex hydride Mg_2NiH_4 is formed with an optical band gap of $E_g \approx 1.6$ eV.[5,6] Mg_2NiH_4 has a cubic structure which transforms to a low symmetry monoclinic phase at $T < 510$ K. In both structures, hydrogen is located in the vicinity to the Ni atoms and the $[NiH_4]^{4-}$ complexes are essentially ionically bound to Mg^{2+}. However, the exact position of the hydrogen atoms is still not resolved.[7] From pressure-composition isotherms at high temperatures the pressure of the phase transition $Mg_2NiH_{0.3}$ to Mg_2NiH_4 can be estimated to occur at 1 Pa at room temperature (RT).[8]

In thin films, the metal-semiconductor transition is reversible[3,9] and can be used to switch optically between a metallic reflecting and semiconducting transparent state. Besides these two "normal" states of a switchable mirror, thin films of Mg_2NiH_x exhibit a third intriguing black state.[9] This state, occurring at intermediate hydrogen concentrations is characterized by a low reflection ($R \leqslant 0.25$) over the entire visible spectrum while transmission is essentially zero. The low reflection and transmission imply a high absorption ($\geqslant 75\%$) of the incoming light. In a first report, Isidorsson *et al.* concluded from a simple Drude model that an unusually large decrease of the free charge carrier density by a factor 25 takes place as hydrogen is incorporated.[9] This idea was, however, in contradiction to the observed low resistivity of Mg_2NiH_x with $x \lesssim 1$. Furthermore, Hall-effect data by Enache *et al.*[10] evidence that each added H-atom removes *one* electron from the conduction band as expected for anionic hydrogen and the formation of $[NiH_4]^{4-}$ complexes. A detailed analysis of the transport data within the framework of an effective medium theory (Bruggeman approximation) showed that the inclusions of the composite system have a peculiar geometry, i.e., they are very flat oblates.[10] The meaning of this result becomes clear in comparison with an advanced analysis of the optical and structural data. Lohstroh *et al.* showed that a black state with $R < 0.25$ and $T < 0.0001$ (at visible light wavelength) cannot be realized by a homogeneous Mg_2NiH_x layer of 200 nm thickness.[11] They found that in thin films, the nucleation of the hydrogen-rich phase $Mg_2NiH_{4-\delta}$ starts preferentially in the vicinity to the film/substrate interface and not, as intuitively expected, close to the catalytic Pd layer at the surface. Consequently, the initially homogeneous $Mg_2NiH_{0.3}$ layer splits spontaneously into a double layer system of $Mg_2NiH_{0.3}$ and $Mg_2NiH_{4-\delta}$ as schematically indicated in Figs. 1(a) and 1(b).

The optical black state is connected to the state sketched in Fig. 1(b): The mixture of metallic and dielectric particles ($Mg_2NiH_{0.3}$ and $Mg_2NiH_{4-\delta}$, respectively) exhibits a very low reflection and an enhanced absorption while transmis-

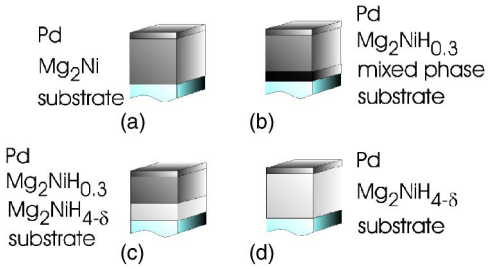

FIG. 1. Schematic picture of the hydrogenation sequence in Mg_2NiH_x films covered with Pd. Upon exposure to hydrogen initially a homogeneous layer Mg_2Ni absorbs hydrogen in solid solution and $Mg_2NiH_{0.3}$ is formed (a). Upon further hydrogen loading the nucleation of the hydrogen-rich phase Mg_2NiH_4 starts in a thin layer of ≈30 nm thickness at the film/substrate interface (b) and a two-layer system is formed spontaneously. In the black state, this mixed layer consists of approximately 20 vol % $Mg_2NiH_{0.3}$ and 80 vol % $Mg_2NiH_{4-\delta}$. When the nucleating layer is fully loaded to $Mg_2NiH_{4-\delta}$ it subsequently grows in thickness (c) until the entire film is loaded to semiconducting, transparent $Mg_2NiH_{4-\delta}$ (d).

sion is effectively suppressed by the remaining metallic layer close to the Pd surface which additionally provides the metallic conductivity of the film. (The photometric measurements are done through the transparent substrate in order to minimize surface roughness effects and the influence of the Pd layer hence the light impinges first at the nucleating $Mg_2NiH_{4-\delta}$ layer.) When the nucleating layer is completely loaded to $Mg_2NiH_{4-\delta}$ it starts to grow [see Fig. 1(c)] until the entire film has switched [see Fig. 1(d)].[11,12]

In this paper we describe the structural, thermodynamic, and optical properties during hydrogenation of Mg_2NiH_x switchable mirrors. From the photometric measurements on Mg_2NiH_x films the dielectric function is inferred for metallic Mg_2NiH_x ($x \lesssim 0.3$) and semiconducting $Mg_2NiH_{4-\delta}$. So far, only a few studies have been devoted to the optical properties of Mg_2Ni and semiconducting Mg_2NiH_x (Refs. 3 and 5) mainly because the hydrides suffer from embrittlement when in bulk form.

Besides the determination of the optical constants, special emphasis is given to the origin of the black state. X-ray diffraction (XRD) and electrochemical loading experiments confirm nicely that it is connected with the onset of the two-phase regime $Mg_2NiH_{0.3}$-$Mg_2NiH_{4-\delta}$ close to the film/substrate interface as previously deduced solely from optical data. Hydrogen profiling with the resonant reaction $^1H(^{15}N,\alpha\gamma)^{12}C$ corroborates the unusual hydrogen loading sequence independently. We show that the optical response can be fully understood by using only $\tilde{\epsilon}_{Mg_2NiH_{0.3}}$ and $\tilde{\epsilon}_{Mg_2NiH_{4-\delta}}$ and the layered structure of the film. We find that the pressure-composition isotherms show a single reaction pressure for the $Mg_2NiH_{0.3}$-$Mg_2NiH_{4-\delta}$ phase transition and we conclude that the substrate interface mainly affects the kinetics of the phase transition. For hydrogen storage applications the identification of the mechanism of the enhanced kinetics is of special interest in order to improve the often sluggish kinetics of Mg-based storage materials.

The paper is organized as follows: In Sec. II the experimental techniques are described. Sec. III presents the experimental findings on the structure and hydrogen concentration in Mg_2NiH_x films and the results are discussed with special emphasis to intermediate hydrogen concentrations, i.e., where the films appear black. In Sec. IV the dielectric functions of Mg_2Ni, $Mg_2NiH_{0.3}$, and $Mg_2NiH_{4-\delta}$ are derived from optical reflection and transmission data and the optical response at intermediate hydrogen concentrations is discussed.

II. EXPERIMENT

The samples are prepared by evaporation in a ultrahigh-vacuum chamber (base pressure $\sim 10^{-8}$ Pa) or by DC magnetron cosputtering from a Mg and Ni source in a vacuum chamber (base pressure $\sim 10^{-6}$ Pa). The thickness of the films is 30–300 nm and the substrates are kept at room temperature during deposition. A Pd capping layer (5–25 nm) is added *in-situ* for oxidation protection and to promote further hydrogen uptake in the subsequent experiments. For optical measurements and x-ray diffraction quartz glass, sapphire or CaF_2 substrates are used whereas for electrolytical loading glass substrates covered with a 180 nm ITO (indium doped tin oxide) layer are used. The conducting (and transparent) ITO layer is necessary to ensure a homogeneous potential and hence a homogeneous H-uptake over the entire surface area during electrochemical loading. In each deposition run a carbon substrate is included for Rutherford backscattering spectrometry (RBS). The composition—as checked with RBS—is homogeneous over the entire sample thickness and Mg:Ni ratios were Mg_yNi (y:1.7–2.6). The structural characterization is performed in a Bruker D8 Discover x-ray diffractometer (Cu-Kα, $\lambda = 1.5418$ Å). For photometric spectrometry in the visible and near infrared a Bruker IFS66 Fourier transform spectrometer is used with an energy range of 0.72 eV–3.5 eV (corresponding to wavelengths 1722 nm–354 nm). The spectrometer is equipped with a reflection and transmission unit with near normal incidence of the incoming beam. In order to minimize the influence of the Pd capping layer and surface roughness, the photometric measurements are done through the transparent substrate. Gas loading experiments are done *in-situ* in both, the spectrometer and the x-ray diffractometer at pressures up to 10^5 Pa H_2. The hydrogen uptake is monitored with a four-point resistivity measurement in a Van der Pauw configuration.[13] Unloading of the films is done at 100 °C in air. Additional reflection and transmission measurements up to 6 eV were done in a Perkin Elmer Lambda 900 diffraction grating spectrometer with an energy range 0.495 eV–6.19 eV ($\lambda = 2500$–200 nm). For electrolytical loading a standard three electrode setup is used with a HgO/Hg reference electrode and a Pt counter electrode in 1 M KOH electrolyte. During the loading, transmission and reflection are measured simultaneously at a fixed wavelength $\lambda = 635$ nm (1.95 eV).

The ^{15}N method[14] is used for depth profiling of hydrogen in the sample, at the Tandem accelerator in Uppsala. The technique is based on the $^1H(^{15}N,\alpha\gamma)^{12}C$ nuclear resonance reaction and provides the depth profile as well as the total amount of hydrogen. For the profiling, the sample is bom-

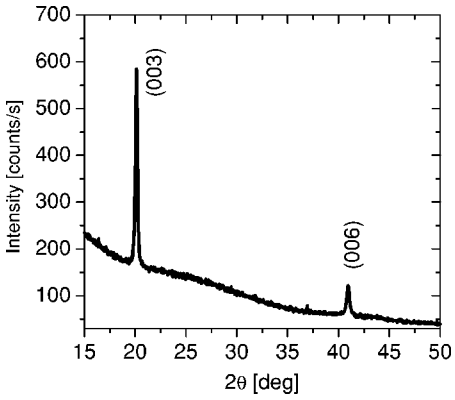

FIG. 2. X-ray diffraction spectra of an as deposited sample 200 nm Mg_2Ni capped with 3 nm Pd. The Mg_2Ni (003) and (006) reflections point to textured growth of the hexagonal lattice with the c axis out of plane. The c-axis lattice parameter ($c=13.23$ Å) is close to the bulk value ($c_{bulk}=13.20$ Å). The background intensity originates form the glass substrate.

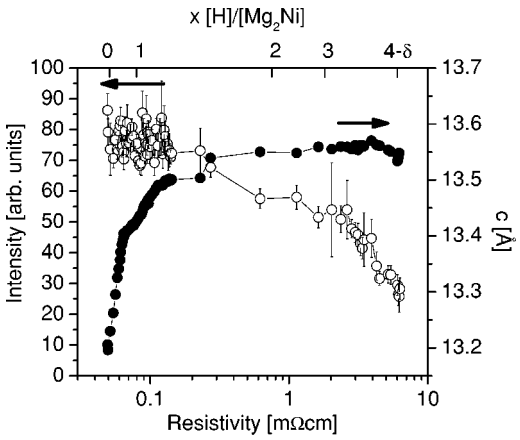

FIG. 3. c-axis lattice parameter (●) and amplitude (○) of the (003) reflection during hydrogen loading. At low hydrogen concentration (i.e., at low resistivity) a linear increase of c is observed. Eventually, c remains constant and the peak intensity starts to diminish around $\rho \approx 0.25$ mΩ cm. The hydrogen concentration (upper scale) is estimated from electrochemical loading experiments.

barded by ^{15}N ions with an energy equal or above the resonance energy (6.385 MeV). Upon penetration, the ions lose energy and, at the depth where the ions have reached the resonance energy, the probability for the reaction is greatly enhanced. The depth resolution is typically 10 Å close to the surface but deteriorates with increasing depth, due to energy straggling. The 4.43 MeV gamma rays are detected in a BGO detector placed at a distance of 3 cm from the sample at an angle of 0 degrees with respect to the incident beam. The diameter of the beam at the surface of the sample is around 1 mm and the beam current (N^{+2}) is typically in the range 10–40 nA. The detection limit is of some atomic ppm and the precision is determined by the counting statistics. The accuracy is governed by the quality of the calibration standard and the accuracy of the calculated stopping power. The values used are from Ziegler[15] and the uncertainty is typically a few percent. Bragg's rule[16] is used for calculating the compound stopping cross section for the hydrogen containing samples. Tantalum hydride ($TaH_{0.47}$) is used as a calibration sample for the absolute hydrogen concentration determination.[17]

III. STRUCTURE AND HYDROGEN CONCENTRATION

A. X-ray diffraction

X-ray diffraction in $\theta-2\theta$ geometry is used to investigate the structure of metallic Mg_2Ni and Mg_2NiH_x at various hydrogen concentrations. In bulk, Mg_2Ni has a hexagonal symmetry with $a=5.216$ Å and $c=13.20$ Å and the lattice mainly expands along the c axis when hydrogen is dissolved in solid solution ($a=5.23$ Å and $c=13.43$ Å).[18]

Figure 2 shows the x-ray diffraction spectra of a 200 nm Mg_2Ni film capped with 3 nm Pd after deposition. Two reflections belonging to hexagonal Mg_2Ni are visible: (003) and (006). The c-axis lattice parameter deduced from the peak positions $2\theta(003)=20.13°$, $2\theta(006)=40.94°$ amounts to $c=13.23$ Å which corresponds within experimental errors to the value observed in bulk. The absence of other reflections indicates textured growth with the c axis of the hexagonal lattice in the direction of the layer normal, but crystallinity is poor as the width of the rocking curve around the (003) reflection is larger than 8°. The width of the reflection in the $\theta-2\theta$ scan implies a coherence length in growth direction of 20 to 30 nm. The coherence length does not change with film thickness indicating that the thickness does not play a major role for the crystal quality.

The structural development during hydrogen uptake is monitored around the (003)-Bragg reflection. Figure 3 shows the lattice parameter and the peak intensity as the hydrogen pressure is increased stepwise up to 0.95×10^5 Pa. The data are plotted as a function of resistivity which is a measure of the hydrogen concentration in the sample.

At low concentrations, i.e., in the solid solution regime $\log\rho\sim x$ and a linear increase of the c axis is observed until a lattice spacing of $c=13.41$ Å is reached at ~0.065 mΩcm. The peak intensity and width remain constant during the expansion hence hydrogen dissolves in the host lattice without changing the crystal symmetry. A comparison with the bulk value for $Mg_2NiH_{0.3}$ ($c=13.43$ Å)[18] and with the electrochemical loading experiments (see Sec. III B) confirms that the solubility range $0\leqslant x\leqslant 0.3$ is only marginally affected by the thin film geometry or the clamping to the substrate. Usually, the adhesion to the substrate strongly influences the hydrogen uptake in thin film and superlattices.[19–21] In the case of Mg_2NiH_x ($0\leqslant x\leqslant 0.3$) the expansion is mainly along the c axis which—in the textured films—can freely expand along the layer normal.

Above $x\approx0.3$ deviations from the linear expansion of the c axis occur and the diminishing intensity of the (003) reflection points to a decreasing $Mg_2NiH_{0.3}$ volume fraction as the two phase region $Mg_2NiH_{0.3}$-$Mg_2NiH_{4-\delta}$ is entered. However, no new reflections appear in the XRD spectra and hence the developing $Mg_2NiH_{4-\delta}$ phase exhibits no long-range coherent order and is either nanocrystalline or amorphous.

In the following we discuss the relation between the structure of Mg_2NiH_x thin films and their optical properties, in

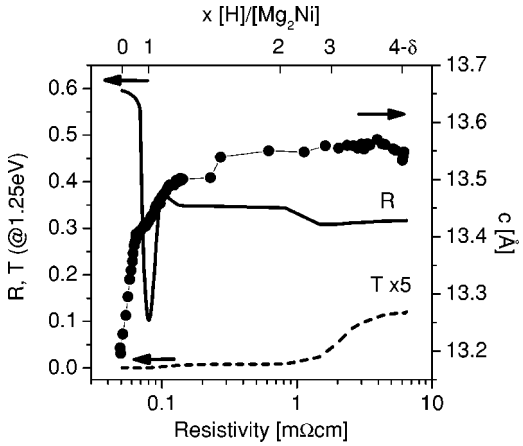

FIG. 4. Comparison of *c*-axis expansion (●) with reflection *R* and transmission *T* (at 1.25 eV) for a sample 200 nm Mg_2Ni capped with 3 nm Pd. In solid solution ($x \lesssim 0.3$), *R* shows metallic reflectivity. At the beginning of the two phase regime $Mg_2NiH_{0.3}$ -$Mg_2NiH_{4-\delta}$ the *c*-axis expansion exhibits a kink and simultaneously *R* decreases dramatically. Transmission is only observed at $x \gtrsim 3.0$. For reasons of clarity *T* is multiplied by a factor 5. The hydrogen concentration (upper scale) is estimated from electrochemical loading experiments.

particular the black state. An example of this optical phenomenon is given in Fig. 4 where the reflection *R* and transmission *T* of a 200 nm thick Mg_2Ni sample capped with 3 nm of Pd are plotted for one fixed energy $\hbar\omega = 1.25$ eV. At low resistivity (i.e., $\rho \lesssim 0.065$ mΩcm, or $x \lesssim 0.3$) the film is shiny metallic with $R \approx 0.6$. Above the solid solution limit small amounts of hydrogen (corresponding to a small increase of ρ) are sufficient for *R* to decrease dramatically whereas *T* remains negligible (too small to be detected, i.e., $T < 10^{-4}$). At this state, *R* is smaller than 0.25 for all wavelength in the visible spectrum and consequently the sample appears black. Further hydrogen uptake yields to a partial recovery of *R* and eventually at $x \gtrsim 3$ the film becomes transparent. The resistivity of the fully loaded semiconducting state ($\rho \approx 6.5$ mΩcm) is mainly limited by the Pd top layer which shortcuts the $Mg_2NiH_{4-\delta}$ film. Obviously, the rapid decrease of *R* to black Mg_2NiH_x coincides with the onset of the two-phase regime $Mg_2NiH_{0.3}$-$Mg_2NiH_{4-\delta}$ which is indicated by the kink in the *c*-axis expansion. However, the intensity of the (003) $Mg_2NiH_{0.3}$ reflection is yet almost unchanged (compare with Fig. 3) hence small amounts of hydrogen above the solid solution limit are sufficient for the pronounced changes in optical appearance. Apparently, the black state is connected with the coexistence of the two phases $Mg_2NiH_{0.3}$ and $Mg_2NiH_{4-\delta}$ and is not an intrinsic property of single phase $Mg_2NiH_{0.3}$.[9] The (003) peak intensity reflects the volume fraction of the remaining $Mg_2NiH_{0.3}$ solid solution phase. With increasing H content the (003) peak intensity and thus the $Mg_2NiH_{0.3}$ layer thickness decreases at the expense of the newly formed $Mg_2NiH_{4-\delta}$ layer. Around $\rho \approx 1$ mΩcm ($x \approx 3$) the $Mg_2NiH_{0.3}$ reflection vanishes rapidly while on the other hand the transmission increases steadily. Eventually, when the film has become fully transparent, the $Mg_2NiH_{0.3}$ (003) reflection cannot be detected any longer and the entire film has switched.

In our films, the crystal structure of semiconducting $Mg_2NiH_{4-\delta}$ could not be resolved. The XRD spectra of the fully loaded samples did not show any additional peaks and presumably the developing hydrogen-rich phase has a very poor crystallinity. Considering the fact that the $Mg_2NiH_{0.3}$ to $Mg_2NiH_{4-\delta}$ phase transition involves a 32% volume expansion and a thorough rearrangement of the atomic positions, it is not surprising that the initially poor crystallinity further deteriorates. Similar results have been reported earlier, both for the structure of $Mg_2NiH_{4-\delta}$ thin films[9,22] and for Mg-Ni-H thin films with higher Mg:Ni ratios (ranging from 4.5:1 to 10:1).[3] Probing the local environment of the Mg atoms by extended x-ray absorption fine structure (EXAFS), Farangis *et al.*[23] found that Mg-Ni films (which were x-ray amorphous after deposition) exhibit order on a microscopic scale up to the second shell neighbors with reduced coordination numbers. The degree of local order decreases with increasing Ni content. After hydrogenation, no EXAFS oscillations could be detected suggesting weak scatterers with a low coordination number located around Mg, and a further deterioration of the crystalline order. Furthermore, the hydrogenation process (in a helium atmosphere with 4% hydrogen) was incomplete in stoichiometric Mg_2Ni thin films, i.e., the signature of metallic Mg_2Ni was still present in the EXAFS spectra.[23] In contrast, our films are at least partially crystalline after deposition even though the grain size is small. After loading in 1.5×10^5 Pa H_2 $Mg_2NiH_{4-\delta}$ exhibit a hydrogen deficiency of $\delta \approx 0.05$.[10] EAXFS at the Ni absorption edge of these films suggests that H is situated in the vicinity to the Ni atoms and $[NiH_4]^{4-}$ clusters are formed.[22] After unloading, the Mg_2Ni-Bragg reflection is partially regained which is presumably due to the heat treatment used in the unloading procedure.

B. Hydrogen concentration and heat of formation

Electrochemical loading is either done in galvanostatic mode with a constant current $I = -50$ μA or by means of the galvanostatic intermittent titration technique (GITT). In the GITT measurements the equilibrium potential U_{eq} is measured as a function of hydrogen concentration. A constant current is applied during a time τ_{p_i}, and subsequently the working electrode (i.e., the Mg_2NiH_x film) is allowed to relax in an open circuit configuration to its equilibrium potential $U_{eq}(x_i)$ at the hydrogen concentration x_i. These steps are repeated until the sample is fully loaded. Typical current pulse times are $\tau_{p_i} = 40$ s with current densities of $j \approx 0.05$ mA/cm^2 and relaxation times $\tau_{r_i} = 180$ s. In a proton donating electrolyte the reaction at the working electrode is

$$H_2O + e^- \rightarrow H_{ad} + OH^- \qquad (1)$$

hence for each transferred electron one H atom is produced that is adsorbed on the Pd surface and subsequently diffuses into the film. From U_{eq} and the Nernst equation (with p_{H_2} in Pa, U_{eq} in volts)

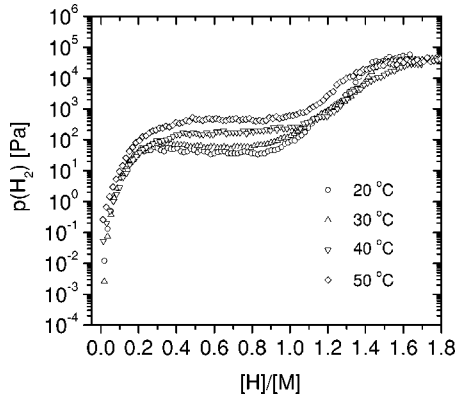

FIG. 5. Pressure composition isotherms of a 200 nm thick $Mg_{1.8}Ni$ film covered with 13 nm Pd at temperatures $T=20\,°C, 30\,°C, 40\,°C$, and 50 °C determined from elctrochemical GITT measurements. With increasing temperature the equilibrium plateau for the $Mg_2NiH_{0.3}$-$Mg_2NiH_{4-\delta}$ phase transition increases from 40 Pa to 460 Pa. [H]/[M] denotes the number of hydrogen atoms per number of metal atoms. (Note that in contrast, the hydrogen concentration x in Mg_2NiH_x refers to the number of hydrogen atoms per formula unit Mg_2Ni.)

$$\ln p_{H_2} = \left(-\frac{2F}{RT}(U_{eq} + 0.926) \right) + 11.51 \qquad (2)$$

the pressure-composition isotherms can be measured. $F=96\,485.3$ C/mol and $R=8.315$ J/mol K denote the Faraday and molar gas constant, respectively.

Figure 5 shows the pressure-composition isotherms of a 190 nm $Mg_{1.8}Ni$ sample covered with 13 nm Pd at temperatures T between 20 °C and 50 °C. The plateau pressure of the $Mg_2NiH_{0.3}$-$Mg_2NiH_{4-\delta}$ phase transition increases with increasing temperature from ≈40 Pa at 20 °C to 460 Pa at 50 °C. From the plateau pressures p_{dis} the heat of formation can be estimated using the van't Hoff equation,[24]

$$\frac{1}{2}\ln p_{dis} = \frac{\Delta H}{RT} - \frac{\Delta S}{R} + 5.75, \qquad (3)$$

where ΔH is the heat of formation and p_{dis} is given in Pa. For metal hydrides, ΔS mainly stems from the entropy loss of gaseous hydrogen. ΔH is obtained from a plot of $\ln p_{dis}$ vs $1/T$. ΔH amounts to $\Delta H=-31.7$ kJ/mol H which agrees well with the value reported for hydrogen absorption in bulk Mg_2Ni ($\Delta H=-32.3$ kJ/mol H).[8,25] At low concentration, when hydrogen is solved in solid solution, the limit is $[H]/[M]\approx 0.16$ at 20 °C. Here, [H]/[M] denotes the number of hydrogen atoms referred to the total number of metal atoms (whereas the hydrogen concentration x gives the hydrogen content per formula unit Mg_2Ni). The observed solid solution limit is slightly higher than the value in bulk $[H]/[M]=0.1$ ($x=0.3$ in $Mg_2NiH_{0.3}$). Above $[H]/[M]\approx 1.0$ the isotherms increase considerably while single phase $Mg_2NiH_{4-\delta}$ is further loaded with hydrogen. The plateau observed at 10^5 Pa is an artifact of the measurement due to hydrogen gas developing at atmospheric pressure.

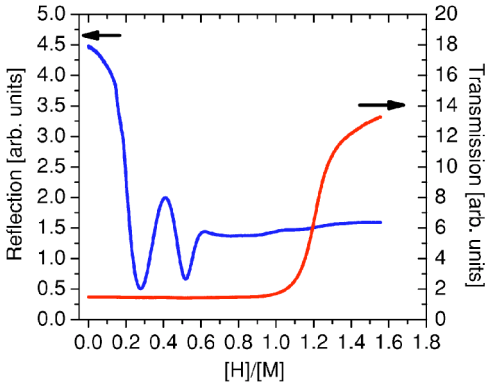

FIG. 6. Reflection R and transmission T of 300 nm $Mg_{1.8}Ni$ covered with 24 nm Pd measured *in-situ* during galvanostatic loading. [H]/[M] denotes the number of hydrogen atoms per metal atom. The oscillating behavior of the reflection is due to interferences of the growing $Mg_2NiH_{4-\delta}$ layer thickness.

During electrochemical loading, reflection and transmission exhibit the same features as in gasochromic loading, i.e., a large decrease of R at low hydrogen concentrations followed by an oscillating behavior and the subsequent onset of transmission. R and T (at $\hbar\omega=1.95$ eV) of a 300 nm thick $Mg_{1.8}Ni$ film covered with 24 nm Pd obtained from galvanostatic loading are shown in Fig. 6. Comparison of these data with those shown in Fig. 4 allows to relate the hydrogen concentration, optical appearance, and resistivity values for characteristic points in the loading cycle. In the solid solution regime R is high and the sample is metallic reflecting. The rapid decrease of R coincides with the beginning of the two-phase region (compare Fig. 5). The minimum of R is associated with an average hydrogen concentration $[H]/[M]\approx 0.27$. At larger hydrogen contents R recovers and even shows a second oscillation which stems from interference of light that is reflected at the two interfaces of the evolving transparent $Mg_2NiH_{4-\delta}$ layer [compare Fig. 1(c)]. This points to an ordered double layering with flat interfaces. In the black state each additional H atom above the solid solution limit is in fact located in a ≈30 nm layer close to the substrate interface (see Sec. III C). If one considers this double layering and recalculates the hydrogen content for the nucleating layer, the concentration amounts to $[H]/[M]\approx 1.12$. This implies that in the black state, the hydrogen concentration close to the film/substrate interface amounts to $x\approx 3.14$ per formula unit $Mg_{1.8}NiH_x$ pointing indeed to a mixture of $Mg_2NiH_{0.3}$ and $Mg_2NiH_{4-\delta}$ (and presumably a small amount of amorphous Mg-Ni of unknown composition) with an approximate atomic ratio of 25:75. The average H concentration in the black state mainly depends on the ratio between the thickness of the composite layer and the metallic layer $Mg_2NiH_{0.3}$ on top. Above $[H]/[M]\approx 1.0$, Mg_2NiH_x becomes transparent.

C. Hydrogen depth profiling

For a direct confirmation of the layered structure of $Mg_2NiH_{0.3}$-$Mg_2NiH_{4-\delta}$ upon hydrogen exposure, a hydrogen depth profile is measured at two stages of the loading pro-

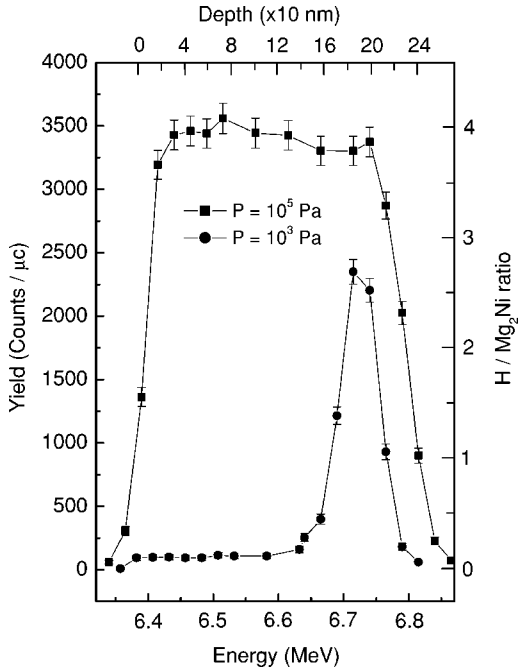

FIG. 7. Hydrogen depth profiling of a 200 nm thick Mg_2Ni film capped with 5 nm Pd. The sample is first hydrogenated at 10^3 Pa to generate the black state (circles) and subsequently exposed to 10^5 Pa to measure the fully loaded sample (squares).

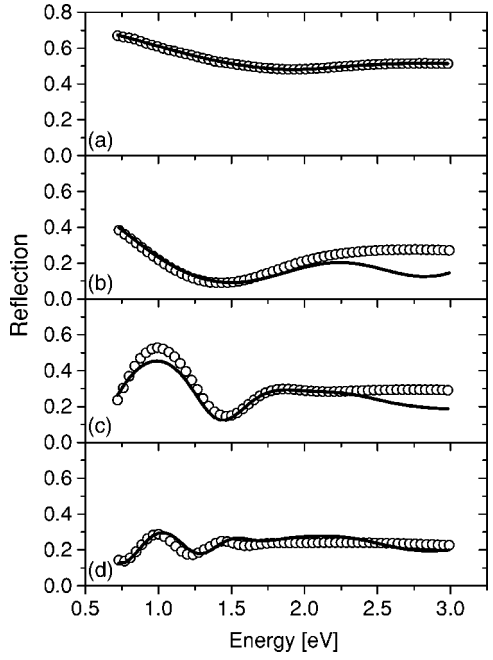

FIG. 8. Reflection (○) for a 250 nm thick $Mg_{1.7}NiH_x$ sample covered with 7 nm Pd at various stages of hydrogen loading. (a) As deposited $Mg_{1.7}Ni$, (b) black $Mg_{1.7}NiH_{\approx 0.8}$, (c) $Mg_{1.7}NiH_{\approx 2.5}$, and (d) transparent $Mg_{1.7}NiH_{\approx 4}$. The solid lines are calculations based on a double layered composition of $Mg_2NiH_{0.3}$ and $Mg_2NiH_{4-\delta}$.

cess, i.e., in the black state and in fully loaded $Mg_2NiH_{4-\delta}$.

Prior to ^{15}N measurements, the sample is loaded in a dedicated H-reaction cell. The black state is obtained by exposing the sample to 10^3 Pa hydrogen pressure at room temperature for approximately 1 hour. The sample is then introduced in the analysis chamber and cooled down to 77 K in order to prevent hydrogen desorption before and during the measurements. Figure 7 shows the results for a 200 nm thick Mg_2Ni sample capped with 5 nm Pd. The hydrogen concentration is plotted as a function of the sample depth, i.e., 0 nm corresponds to the Pd surface. In the black state, the hydrogen concentration has a maximum around 180 nm, i.e., close to the film/substrate interface while the rest of the sample only exhibits a very small H content. The hydrogen rich layer extends approximately over 50 nm and the concentration (per Mg_2Ni) is $x \approx 2.7$ at its maximum. After this first ^{15}N measurement, the sample is removed from the chamber and visually inspected. No change in the color of sample can be detected when looking from the substrate side, indicating that the black state remains after the measurement. A second measurement is taken after the sample is exposed to 10^5 Pa of hydrogen in the H reaction cell during one week and the results are also plotted in Fig. 7 (squares). The hydrogen concentration of the fully loaded sample is indeed homogeneous over the entire film thickness and close to $x \approx 4$. The expansion of the hydrogen profile to higher energies (i.e., larger depth) reflects the increasing layer thickness (by approximately 15%) during hydrogen uptake.

IV. OPTICAL CONSTANTS

For a quantitative understanding of the hydrogen concentration dependence of the optical properties of inhomogeneous Mg_2NiH_x it is necessary to know the optical constants of Mg_2Ni, $Mg_2NiH_{0.3}$, and $Mg_2NiH_{4-\delta}$. Figure 8 shows typical reflection spectra of the different optical states during H loading, for a sample $Mg_{1.7}NiH_x$ capped with 7 nm Pd. Metallic $Mg_{1.7}Ni$ has a reflection R ranging from $R \approx 0.4$–0.65 in the studied energy range [Fig. 8(a)]. After hydrogen is introduced, $Mg_{1.7}NiH_x$ becomes black [Fig. 8(b)] with $R < 0.25$ and essentially zero transmission over the entire visible spectrum ($1.58\ \text{eV} \leqslant \hbar\omega \leqslant 3.26\ \text{eV}$). Further loading yields to a recovery of R as transparent $Mg_2NiH_{4-\delta}$ grows in thickness and interference fringes appear in the spectrum that shift to lower energies with increasing hydrogen concentration [Fig. 8(c)] until eventually the sample is fully loaded [Fig. 8(d)] and transparent.

Reflection and transmission spectra are used to determine the dielectric function of the single phase compositions Mg_2Ni, $Mg_2NiH_{0.3}$, and $Mg_2NiH_{4-\delta}$. The optical response at intermediate hydrogen concentrations can then be calculated for a two layer model.

A Drude-Lorentz parametrization is used to describe the complex dielectric function $\tilde{\epsilon} = \epsilon_1 + i\epsilon_2$,

$$\tilde{\epsilon} = \epsilon_\infty - \frac{\omega_p^2}{\omega^2 + i\omega\Gamma} + \sum_{j=1}^{N} \frac{f_j}{\omega_{0j}^2 - \omega^2 - i\omega\beta_j}. \qquad (4)$$

The first term (Drude term) with the plasma frequency ω_p and damping term $\Gamma = 1/\tau$, where τ is the relaxation time, describes the contribution from free electrons. The plasma frequency is related to the free charge carrier density n_{opt} by $\omega_p^2 = n_{\text{opt}} e^2/\epsilon_0 m$, where e and m are the electron charge and mass, respectively. Experimentally, ω_p can be determined

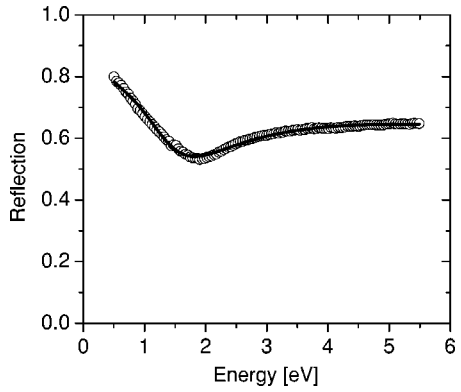

FIG. 9. Reflection R of a 100 nm thick $Mg_{1.8}Ni$ film capped with 5 nm Pd (○) measured through the substrate. The solid line is a calculation using the parameters from Table I.

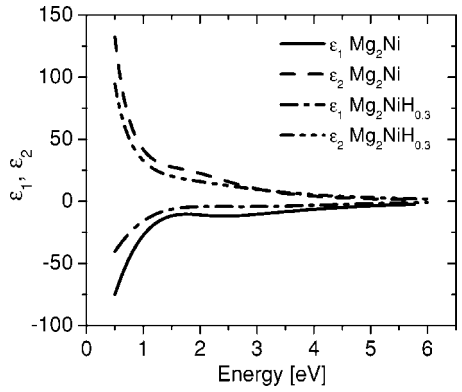

FIG. 10. Real (ϵ_1) and imaginary (ϵ_2) part of the dielectric function obtained from fits to the measured reflection and transmission data of metallic Mg_yNi and $Mg_yNiH_{0.3}$ (y:1.8–2.2).

from the energy where ϵ_1 crosses zero. The second term arises from bound electrons. The Lorentz oscillators are characterized with an oscillator strength f_j, a resonance frequency ω_{0j} and a damping term β_j. N gives the number of Lorentz oscillators, which varied between $N=1$ for metallic Mg_2Ni to $N=3$ for semiconducting $Mg_2NiH_{4-\delta}$. ϵ_∞ takes all excitations at higher energies into account. $\tilde{\epsilon}$ is connected to the complex index of refraction $\tilde{n}=n+ik$ by

$$\epsilon_1 = n^2 - k^2, \tag{5}$$

$$\epsilon_2 = 2nk, \tag{6}$$

where n is the refractive index and k the extinction coefficient. R_{cal} and T_{cal} of the entire layered stack (substrate-Mg_2NiH_x-PdH_x) are calculated using a transfer matrix method that considers the Fresnel reflectance and transmittance coefficients at each interface and the absorption in each layer.[26] n and k of PdH_x and the substrate, necessary for such a calculation, are taken from Refs. 27 and 28, respectively, and the thickness of the layers is determined from RBS measurements. To extract $\tilde{\epsilon}$, the Drude-Lorentz parameters of the Mg_2NiH_x layer are optimized so as to minimize the difference between the calculated values R_{cal} and T_{cal} and the measured results. The used parametrization has the advantage that the fitted $\tilde{\epsilon}$ satisfies the Kramers-Kronig relations. The solution is thus intrinsically satisfying causality.[29] Since the films expand upon hydrogenation the thickness of the loaded films is also taken as a fit parameter. The fits indicate typical expansions between 10% and 20%. Similar values for the increase in thickness have been found by means of small angle x-ray reflectometry and hydrogen depth profiling (see Fig. 7). This expansion is less than expected from bulk (32 vol %). In clamped thin films the expansion can only be along the layer normal and hence the film thickness should increase by 32%. The discrepancy is most likely due to a disordered structure and a nonideal clamping of the film.

A. Metallic Mg_2Ni

Figure 9 shows an example for the reflection of $Mg_{1.8}Ni$ in the as-prepared state. For metallic Mg_yNi it is sufficient to consider only the free electron term and one Lorentz oscillator, i.e., $N=1$ in Eq. (4). The calculated result for the optimized $\tilde{\epsilon}$ is shown in Fig. 9. For all the investigated samples (sputtered or evaporated with different thicknesses) $\tilde{\epsilon}$ of metallic Mg_yNi obtained from such an analysis is quite similar although small differences are observed which most likely stem from variations in composition. Especially ϵ_1 is smaller for samples with higher Mg content (up to a Mg:Ni ratio of 4:1). Such a behavior can be expected from a comparison between $\tilde{\epsilon}_{Mg}$ and $\tilde{\epsilon}_{Ni}$ of the pure metals. The *s*-valence electrons of Mg make it a very good Drude metal whereas the *d*-electrons in Ni give rise to interband transitions which screen the plasma energy. As a result ϵ_1 crosses the zero level at energies well below $\omega_p = n_{opt}e^2/\epsilon_0 m$ expected from the free charge carrier density n_{opt}. Experimentally this can be observed in the gradually decreasing R of pure Ni at energies smaller than the plasma energy ω_p.

For our analysis we concentrate on compositions close to stoichiometric Mg_2Ni. In Fig. 10 ϵ_1 and ϵ_2 for Mg_yNi (y: 1.8–2.2) are plotted and the corresponding Drude-Lorentz parameters are given in Table I.

From the plasma energy $\hbar\omega_p = 8.14$ eV and the damping term Γ the optical charge carrier density n_{opt} and the scattering time $\tau = 1/\Gamma$ can be inferred. They amount to $n_{opt} = 4.8 \times 10^{22}$ cm^{-3} and $\tau = 9.9 \times 10^{-16}$ s, respectively. These values are in agreement with the values obtained from DC electrical transport measurements[10] ($n_{dc} = 8.7 \times 10^{22}$ cm^{-3} and $\tau = 9 \times 10^{-16}$ s) even though these values have been measured at $\hbar\omega = 0$.

TABLE I. Drude-Lorentz parameters of the effective dielectric function [Eq. (4)] of Mg_yNi and $Mg_yNiH_{0.3}$ ((y: 1.8–2.2). All parameters are in eV except ε_∞ which is dimensionless.

Parameter	Mg_yNi (y: 1.8–2.2)	$Mg_yNiH_{0.3}$ (y: 1.8–2.2)
ε_∞	2.08±0.51	2.72±2.99
ω_p	8.14±0.48	7.03±1.34
$1/\Gamma$	1.50±0.31	1.28±0.44
$\sqrt{f_1}$	9.21±0.20	10.16±1.77
ω_{01}	2.13±0.16	2.56±0.40
β_1	2.36±0.38	3.94±1.68

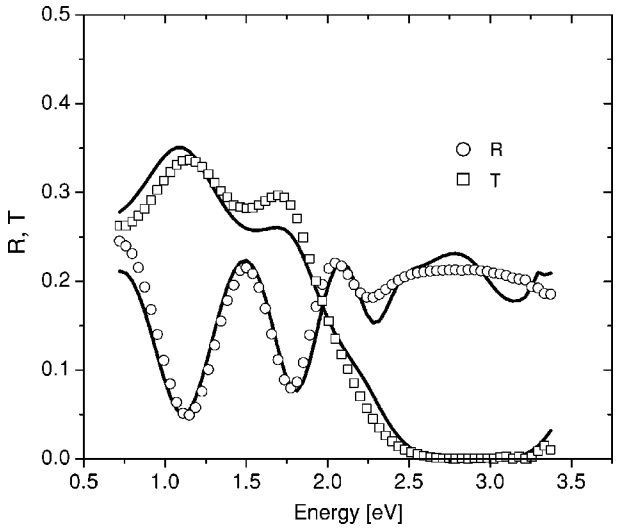

FIG. 11. R (○) and T (□) for a 210 nm thick $Mg_{2.55}Ni$ film capped with 6 nm of Pd after loading in 10^5 Pa H_2. The solid lines are the R_{cal} and T_{cal} for the fitted ϵ_1 and ϵ_2 given in Fig. 12(c).

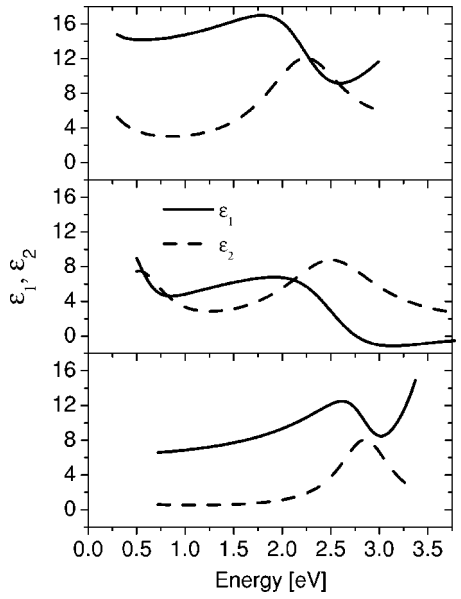

FIG. 12. Real part ϵ_1 (solid line) and imaginary part ϵ_2 (dashed line) of the dielectric function for (a) $Mg_{1.7}Ni$, (b) $Mg_{1.8}Ni$, and (c) $Mg_{2.55}Ni$, after loading in 10^5 Pa H_2 at room temperature.

The second column in Table I gives the Drude-Lorentz parameters of the metallic solid solution phase ($Mg_yNiH_{x\approx 0.3}$) that are obtained from a similar analysis. The probed energy range for these measurements is $0.72 \leqslant \hbar\omega \leqslant 3.5$ and ϵ_1 and ϵ_2 for $Mg_yNiH_{0.3}$ (y: 1.8–2.2) shown in Fig. 10 are extrapolated to higher energies. The decreasing charge carrier density upon exposure to hydrogen is reflected in the plasma energy which decreases from $\hbar\omega_p = 8.14$ eV to 7.03 eV. ϵ_1 is slightly less negative than in the pure phase.

B. Semiconducting Mg_2NiH_4

The optical constants of semiconducting $Mg_yNiH_{4-\delta}$ (y: 1.7–2.55) are determined from samples loaded in 10^5 Pa hydrogen at room temperature. For a good fit it is necessary to consider three Lorentz oscillators, i.e., $N=3$ in Eq. (4), and for some samples it is even necessary to take an additional layer at the Pd-Mg_2Ni interface into account. This is not surprising since the formation of an interface alloy in Mg-Pd layer systems is well known[30] and that layer combined with surface oxidation might hamper the hydrogen uptake.[27,31]

Figure 11 shows R and T for a 210 nm thick $Mg_{2.55}NiH_{4-\delta}$ film covered with 6 nm Pd. The solid lines show the results of the fitting and the corresponding ϵ_1 and ϵ_2 are given in Fig. 12(c). In the fully loaded state we observe ≈30% transparency. In the vicinity of the absorption edge (i.e., in the interference-free region) the transmission follows:[27]

$$\ln T = \ln T_0 - C\frac{(\hbar\omega - E_g)^{\nu}}{\hbar\omega}, \tag{7}$$

where E_g is the band gap, C is a constant, and T_0 contains the transmission of the substrate and the Pd cap layer. Depending on the type of transitions ν takes different values: for direct, allowed (forbidden) transitions $\nu=\frac{1}{2}$ ($\nu=\frac{3}{2}$) and for indirect allowed (forbidden) transitions $\nu=2$ ($\nu=3$). For our nanocrystalline or amorphous films $\nu=2$ is used, as it has been reported to give the best results for amorphous or nanocrystalline materials.[32] Around the absorption edge T_0 and C are approximately constant and a fit to Eq. (7) gives $E_g \approx 1.8$ eV for $Mg_{2.55}NiH_{4-\delta}$. This is in agreement with the values reported earlier for $Mg_yNiH_{4-\delta}$ ($y \geqslant 2$) with excess Mg.[6] The fitted dielectric function reflects the semiconducting behavior of $Mg_2NiH_{4-\delta}$ [see Fig. 12(c)]. At energies above the band gap ϵ_2 exhibits a maximum that describes the onset of absorption. In Figs. 12(a)–12(c) ϵ_1 and ϵ_2 of $Mg_yNiH_{4-\delta}$ are shown for three different Mg:Ni ratios. While the basic shape of the dielectric function remains the same, the absorption edge and hence E_g shifts to higher energies with increasing Mg content. From Eq. (7) E_g amounts approximately to 1.3 eV for $Mg_{1.7}NiH_{4-\delta}$ and $Mg_{1.8}NiH_{4-\delta}$ shown in Figs. 12(a) and 12(b). Myers *et al.* calculated the dielectric function from LDA band structure calculations for LT-Mg_2NiH_4 and HT-Mg_2NiH_4 for three different hydrogen configurations, i.e., a square planar, a distorted tetrahedron and a perfect tetrahedral arrangement around the Ni atoms.[33] For all structures (except for the square planar configuration which is metallic) they found the band gap to be indirect, and in dependence of the structure the optical gaps are in between 1.9 to 2.4 eV which is slightly higher than our experimental values. For all studied compositions, ϵ_2 does not vanish at energies below E_g which is presumably caused by incomplete loading or structural defects that generate impurity states in the band gap.

C. Intermediate hydrogen concentrations

In Figs. 8(a) and 8(d) R is plotted for the two limiting cases of single phase (i) Mg_2Ni and (ii) $Mg_2NiH_{4-\delta}$.[34] The solid lines give R_{cal} from the fitting procedure. In contrast Figs. 8(b) and 8(c) depict R at intermediate hydrogen con-

centrations. For $Mg_2NiH_{4-\delta}$ with $0.3<x<4-\delta$ we find that it is not possible to fit the optical data if one assumes a homogeneous hydrogen uptake in the Mg_2Ni layer.[11] It can be shown that, assuming a homogeneous Mg_2NiH_x layer (with the inclusions smaller than the wavelength of light) there exists no pair (n,k) that can reproduce simultaneously the measured R and T.[11] The optical response at intermediate hydrogen concentration can, however, be fully understood if the double layer structure of the sample is taken into account.

The spectra shown in Figs. 8(b) and 8(c) correspond to states illustrated in Figs. 1(b) and 1(c). In Fig. 1(b) $Mg_2NiH_{4-\delta}$ starts to nucleate in a thin layer close to the substrate. This thin layer consists of metallic $Mg_2NiH_{0.3}$ and semiconducting $Mg_2NiH_{4-\delta}$. Its dielectric function $\langle\tilde{\epsilon}\rangle$ can be described by an effective medium theory if the grain size of the respective particles is smaller than the wavelength of light. In a simple approach, we use Bruggeman's approximation for spherical particles although we have no detailed knowledge of the microstructure in our films. $\langle\tilde{\epsilon}\rangle$ is implicitly given by[35]

$$f^A\frac{\tilde{\epsilon}_A-\langle\tilde{\epsilon}\rangle}{\tilde{\epsilon}_A+2\langle\tilde{\epsilon}\rangle}+f_B\frac{\tilde{\epsilon}_B-\langle\tilde{\epsilon}\rangle}{\tilde{\epsilon}_B+2\langle\tilde{\epsilon}\rangle}=0 \tag{8}$$

$f_{A,B}$ and $\tilde{\epsilon}_{A,B}$ are the volume fraction and the complex dielectric function of the metallic $(A, Mg_2NiH_{0.3})$ and the semiconducting $(B, Mg_2NiH_{4-\delta})$ phase, respectively. In Fig. 8(b) Eq. (8) is applied for a mixture 20 vol % $Mg_2NiH_{0.3}$–80 vol % $Mg_2NiH_{4-\delta}$ to obtain $\langle\tilde{\epsilon}\rangle$ of the 30 nm nucleation layer, and subsequently R of the entire stack is calculated (solid lines). The agreement between experiment and calculation confirms that the formation of a ≈30 nm thin, mixed layer $Mg_2NiH_{0.3}$-$Mg_2NiH_{4-\delta}$ at the film/substrate interface can indeed explain the black state. The discrepancy between calculation and measured data at higher energies is presumably due to the not ideally flat interface between the two evolving layers. In the optical calculation the interface roughness is not considered. As more hydrogen is introduced a uniform transparent layer of $Mg_2NiH_{4-\delta}$ is formed which subsequently grows in thickness. As a result, interference fringes appear in the spectra due to multiple reflection of light at the interfaces of the transparent $Mg_2NiH_{4-\delta}$ layer. This is demonstrated in Fig. 8(c) where R_{cal} is obtained for a double layer 130 nm $Mg_2NiH_{0.3}$ and 120 nm $Mg_2NiH_{4-\delta}$ covered with 7 nm of PdH_x. Further confirmation of the double layer structure is obtained from reflection measurements with the light impinging first on the Pd top layer.[11] In these measurements, which mainly probe the part of the sample close to the surface, and R remains high up to large hydrogen concentrations $(x\geqslant 3)$.

D. Comparison with DC transport measurements

Temperature dependent DC resistivity and Hall-effect data by Enache *et al.*[10] showed that the charge carrier density n_{dc} (obtained form Hall-effect measurements) decreases linearly with increasing hydrogen concentration x. In solid solution, i.e., for $x\leqslant 0.3$ the optical data reflect these results: the plasma energy decreases linearly from $\hbar\omega=8.14$ eV in the metal to $\hbar\omega=7.03$ eV and correspondingly the optical charge carrier density n_{opt} decreases as well. The transport data show that the linear relation between n_{dc} and x holds for the entire concentration range $0\leqslant x\leqslant 4$ although a two-component composite system $Mg_2NiH_{0.3}$-$Mg_2NiH_{4-\delta}$ is formed above $x\geqslant 0.3$.[10] This is in agreement with the anionic hydrogen model where each hydrogen removes one electron from the conduction band to form negatively charged $[NiH_4]^{4-}$ complexes. However, above $x\geqslant 0.3$, the analogy between DC-transport results and the optical measurements is less obvious due to the self-organized layering of the film in the two phase regime. Reflection mainly probes the region close to the film/substrate interface (since it is measured through the substrate) while resistivity and Hall-effect data are averages over the entire film thickness. In the black state, R thus mainly reflects the two phase regime Mg_2Ni -$Mg_2NiH_{4-\delta}$ of the nucleating layer while the electrical transport data are dominated by the remaining metallic layer close to the surface. Consequently, Hall - effect and resistivity data can be analyzed in an effective medium theory over the entire two phase regime while this is not possible for the optical data. This analysis reveals that the inclusions have a very peculiar geometry, i.e., they are very flat oblates with an axis ratio between 10 and 20.[10] The extreme limit of this geometry are flat sheets, in full agreement with the layered structure that was confirmed by H - depth profiling and the optical and structural data presented above.

E. Comparison with MgRE (rare earth) thin films

Thin films of Mg_2Ni are not the only switchable mirrors that exhibit a highly absorbing state. When loaded with hydrogen, MgRE (RE: Y, La, Gd)[2,36] thin films and Mg[37] show similar absorption levels. Upon the first exposure to hydrogen, MgRE disproportionates into REH_2 and Mg. Both constituents take up hydrogen and both change their optical appearance.[27,38] After the initial disproportionation, the reversible switching takes place between metallic Mg-REH_2 and transparent MgH_2-$REH_{3-\delta}$. At intermediate hydrogen concentrations, $MgREH_x$ exhibits ≈80% absorption of the incoming light, similar to the values that have been obtained in Mg_2NiH_x. Despite these apparent similarities the mechanism for the black state in Mg_2NiH_x is distinctively different from that in $MgREH_x$ switchable mirrors. In $MgREH_x$ it is directly connected to the broadening of the surface plasmon spectrum at the percolation threshold of the metal-insulator transition similar to the well-studied cluster systems Ag-glass,[39] Au-glass[40] or Co-Al_xO_3.[35] It has been shown[37] that the key ingredient is the coexistence of Mg and MgH_2 nanograins that are homogeneously dispersed over the entire film thickness and the photometric measurements are well described using effective dielectric constants for a mixture of Mg and MgH_2 small particles.

In contrast, the most important ingredient for the black state in Mg_2NiH_x thin films is the self - organized double layer formation. The initial nucleation of $Mg_2NiH_{4-\delta}$ takes place in a small layer close to the substrate. Essential for the high absorption in Mg_2NiH_x are thus the optical properties of that mixed layer in the vicinity of the film-substrate inter-

face, the interference of light reflected at the two interfaces of this weakly transparent layer which results in a broad reflection minimum and the remaining metallic $Mg_2NiH_{0.3}$ on top that suppresses any transmission [compare Fig. 1(b)].

V. CONCLUSIONS

The structural and optical properties of Mg_2NiH_x thin films covered with Pd are systematically studied upon hydrogen loading in order to develop a quantitative understanding of the intriguing black state and interference effects observed recently in this system.[11,12] Similar to bulk Mg_2NiH_x, the hydrogen solid solution limit is $x \approx 0.3$. Further hydrogen loading yields to the formation of $Mg_2NiH_{4-\delta}$ which is accompanied by a structural phase transition and a large volume increase.

Analysis of the optical reflection and transmission data shows that the high optical absorption (black state) at relatively low hydrogen concentrations ($[H]/[M] \approx 0.27$) is due to a mixture of $Mg_2NiH_{0.3}$ and $Mg_2NiH_{4-\delta}$ particles in the vicinity of the film/substrate interface while the material in the upper layer remains metallic $Mg_2NiH_{0.3}$. This unusual loading sequence is confirmed by ^{15}N hydrogen - depth profiling which shows that in the black state hydrogen is almost exclusively located in the vicinity to the substrate interface. The width of the hydrogen rich layer is ≈ 50 nm in good agreement with ≈ 30 nm estimated from the photometric data. X-ray diffraction and electrochemical loading results support these findings and clear evidence is obtained that the black state is connected to the onset of $Mg_2NiH_{4-\delta}$ nucleation.

The dielectric functions of the homogenous phases Mg_2Ni, $Mg_2NiH_{0.3}$, and $Mg_2NiH_{4-\delta}$ are determined. In the two metallic states $\tilde{\epsilon}$ is fairly robust against small variations in composition and the optical free charge density fits well with the value obtained from transport measurement. In contrast, the optical properties of semiconducting $Mg_yNiH_{4-\delta}$ (y: 1.7–2.6) vary considerably with the Mg:Ni ratio. Using $\tilde{\epsilon}_{MgyNiH_{0.3}}$ and $\tilde{\epsilon}_{MgyNiH_{4-\delta}}$, the two layer model explains reflection and transmission at all intermediate hydrogen concentrations.

Although the nucleation of $Mg_2NiH_{4-\delta}$ starts preferentially near the substrate there is no indication for an additional plateau pressure at hydrogen concentrations close to the black state. We conclude that the substrate/film interface thus mainly influences the kinetics of the hydrogen uptake. The robustness of the black state concerning composition, choice of substrate and loading conditions (i.e., gas phase or electrolytical loading) and the fact that Mg_2CoH_x exhibits similar optical properties, suggest that it is an intrinsic property of these films. The microscopic mechanism leading to the intriguing self-organized layering is also of special interest for the catalysis of hydrogen sorption in the complex metal hydrides storage materials such as Mg_2NiH_x, Mg_2CoH_x, and Mg_2FeH_x.

ACKNOWLEDGMENTS

The authors thank I. A. M. E. Giebels and J. Isidorsson for fruitful discussions. J. H. Rector is acknowledged for technical support. This work is part of the research program of the Stichting voor Fundamenteel Onderzoek der Materie (FOM), financially supported by the Nederlandse Organisatie voor Wetenschappelijk Onderzoek (NWO).

*Corresponding author; email: lohstroh@nat.vu.nl

[1] J. N. Huiberts, R. Griessen, J. H. Rector, R. J. Wijngaarden, J. P. Decker, D. G. de Groot, and N. J. Koeman, Nature (London) **380**, 231 (1996).
[2] P. van der Sluis, M. Ouwerkerk, and P. A. Duine, Appl. Phys. Lett. **70**, 3356 (1997).
[3] T. J. Richardson, J. L. Slack, R. D. Armitage, R. Kostecki, B. Farangis, and M. D. Rubin, Appl. Phys. Lett. **78**, 3047 (2001).
[4] T. J. Richardson, J. L. Slack, B. Farangis, and M. D. Rubin, Appl. Phys. Lett. **80**, 1349 (2002).
[5] D. Lupu, R. Sârbu, and A. Biriş, Int. J. Hydrogen Energy **12**, 1987 (1987).
[6] J. Isidorsson, I. A. M. E. Giebels, M. Di Vece, and R. Griessen, Proc. SPIE **4458**, 128 (2001).
[7] G. N. García, J. P. Abriata, and J. O. Sofo, Phys. Rev. B **59**, 11 746 (1999).
[8] J. J. Reilly and R. H. Wiswall, Inorg. Chem. **7**, 2254 (1968).
[9] J. Isidorsson, I. A. M. E. Giebels, R. Griessen, and M. Di Vece, Appl. Phys. Lett. **80**, 2305 (2002).
[10] S. Enache, W. Lohstroh, and R. Griessen, Phys. Rev. B **69**, 115326 (2004).
[11] W. Lohstroh, R. J. Westerwaal, B. Noheda, S. Enache, I. A. M. E. Giebels, B. Dam, and R. Griessen, Phys. Rev. Lett (to be published).
[12] J. L. M. van Mechelen, B. Noheda, W. Lohstroh, R. J. Westerwaal, J. H. Rector, B. Dam, and R. Griessen, Appl. Phys. Lett. **84**, 3651 (2004).
[13] L. J. van der Pauw, Philips Res. Rep. **13**, 1 (1958).
[14] W. Lanford, H. Trautvetter, J. Ziegler, and J. Keller, Appl. Phys. Lett. **28**, 566 (1976).
[15] J. F. Ziegler, "The stopping and ranges of ions in matter," *Handbook of Stopping Cross-Sections for Energetic Ions in all Elements* (Pergamon, New York, 1980), Vol. 5.
[16] W. K. Chu, J. W. Mayers, and M. A. Nicolet, *Backscattering Spectrometry* (Academic, New York, 1978).
[17] B. Hjörvarsson, H. Ryden, T. Ericsson, and E. Karlsson, Nucl. Instrum. Methods Phys. Res. B **42**, 257 (1989).
[18] J. Schefer, P. Fischer, W. Hälg, F. Stucki, L. Schlappbach, J. J. Didisheim, K. Yvon, and A. F. Andresen, J. Less-Common Met. **74**, 1980 (1980).
[19] H. Zabel and A. Weidinger, Comments Condens. Matter Phys. **17**, 239 (1995).
[20] V. Leiner, H. Zabel, J. Birch, and B. Hjörvarsson, Phys. Rev. B **66**, 235413 (2002).

[21] S. Olsson, B. Hjörvarsson, E. B. Svedberg, and K. Umezawa, Phys. Rev. B **66**, 155433 (2002).
[22] M. Di Vece, A. M. J. van der Erden, D. Grandjean, R. J. Westerwaal, W. Lohstroh, J. J. Kelly, and D. C. Koningsberger (unpublished).
[23] B. Farangis, P. Nachimuthu, T. J. Richardson, J. L. Slack, R. C. C. Perera, E. M. Gullikson, D. W. Lindle, and M. Rubin, Phys. Rev. B **67**, 085106 (2003).
[24] R. Griessen and T. Riesterer, *Topics in Applied Physics: Hydrogen in Intermetallic Compounds I* (Springer-Verlag, Berlin, Heidelberg, 1988), p. 219.
[25] S. Orimo and H. Fujii, Appl. Phys. A: Mater. Sci. Process. **78**, 167 (2001).
[26] M. Born and E. Wolf, *Principles of Optics* (Cambridge University Press, Cambridge, 1980).
[27] J. Isidorsson, I. A. M. E. Giebels, H. Arwin, and R. Griessen, Phys. Rev. B **68**, 115112 (2003).
[28] E. D. Palik, *Handbook of Optical Constants of Solids* (Academic, San Diego, 1998).
[29] F. Wouten, *Optical Properties of Solids* (Academic, New York, London, 1972).
[30] A. Krozer, A. Fischer, and L. Schlapbach, Phys. Rev. B **53**, 13 808 (1996).
[31] P. Hjort, A. Krozer, and B. Kasemo, J. Alloys Compd. **237**, 74 (1995).
[32] E. A. Davis and N. F. Mott, Philos. Mag. **22**, 903 (1970).
[33] W. R. Myers, L.-W. Wang, T. J. Richardson, and M. D. Rubin, J. Appl. Phys. **91**, 4879 (2002).
[34] The stoichiometry is actually Mg:Ni=1.7, hence some amorphous Mg-Ni of unknown composition will also be present.
[35] G. A. Niklasson and C. G. Granqvist, J. Appl. Phys. **55**, 3382 (1984).
[36] J. Isidorsson, I. A. M. E. Giebels, E. S. Kooij, N. J. Koeman, J. H. Rector, A. T. M. van Gogh, and R. Griessen, Electrochim. Acta **46**, 2179 (2001).
[37] I. A. M. E. Giebels, J. Isidorsson, and R. Griessen, Phys. Rev. B **69**, 205111 (2004).
[38] A. T. M. van Gogh, D. G. Nagengast, E. S. Kooij, N. J. Koeman, J. H. Rector, R. Griessen, C. F. J. Flipse, and R. J. J. G. A. M. Smeets, Phys. Rev. B **63**, 195105 (2001).
[39] C. G. Granqvist and O. Hunderi, Phys. Rev. B **18**, 2897 (1978).
[40] F. Brouers, J. P. Clerc, G. Giraud, J. M. Laugier, and Z. A. Randriamantany, Phys. Rev. B **47**, 666 (1993).